Measurement of chromatic *X*-*Y* coupling

Y. Ohnishi,* K. Ohmi, H. Koiso, M. Masuzawa, A. Morita, K. Mori, K. Oide, Y. Seimiya, and D. Zhou

High Energy Accelerator Research Organization, KEK, Oho 1-1, Tsukuba, Ibaraki 305-0801, Japan

(Received 7 August 2009; published 28 September 2009)

We have measured and corrected chromatic *X*-*Y* coupling at an interaction point to improve the luminosity of KEKB. We have measured the beam position of betatron oscillations induced by the kicker using turn-by-turn beam position monitors. A phase space structure reconstructed by the beam position provides us not only the Twiss parameters but also information regarding *X*-*Y* coupling. We have also determined chromatic *X*-*Y* coupling using the measured *X*-*Y* coupling at each momentum deviation from the designed beam energy. Skew sextupole magnets are used to correct the chromatic *X*-*Y* coupling.

DOI: 10.1103/PhysRevSTAB.12.091002 PACS numbers: 29.20.db

I. INTRODUCTION

KEKB [1,2] is an asymmetric-energy and a double-ring collider that consists of an 8 GeV electron ring (HER) and a 3.5 GeV positron ring (LER). In the case of a study on elementary processes in the B-physics experiment, a 1.5 T detector solenoid magnet is used to measure the charged decayed particles originating from the vicinity of an interaction point (IP). An antisolenoid magnet is installed behind a final focus quadrupole magnet (QCS) to compensate for the detector solenoid field acting along the beam line. Skew quadrupole magnets are also used to correct *X*-*Y* coupling to be zero at the IP in an ideal lattice.

Optics corrections [3,4] such as horizontal and vertical dispersions, beta functions, and *X*-*Y* coupling have been carried out at the designed beam energy. As a result of beta corrections, the rms of the deviations from the model lattice is typically 5%–10%. In the case of dispersions, the rms of the deviations from the model lattice is $\Delta\eta \sim$ 10 mm in the horizontal and vertical plane, respectively. The averaged rms of the vertical orbits is 15–20 μm after *X*-*Y* coupling correction, when several types of horizontal closed orbit distortions are induced by each horizontal steering magnet. These optics corrections are global and not specific to an IP. Furthermore, it is necessary to adjust *X*-*Y* coupling and dispersion at the IP by using a knob which consists of a local bump orbit at sextupole magnets in order to optimize luminosity during a physics operation (luminosity run). Therefore, it is necessary to perform an independent measurement of the optical parameters at the IP and important to maximize the luminosity performance of the KEKB.

Recently, from the results of computer simulation with beam-beam interactions [5,6], it was found that large chromatic *X*-*Y* coupling at the IP deteriorates the luminosity. A measurement technique and a correction scheme of chromatic *X*-*Y* coupling at the IP have been proposed. The measurement is based on a free betatron oscillation induced by a kicker. The beam positions over 1000 consecutive turns are detected by turn-by-turn beam position monitors (BPMs) [7,8] placed on either side of the IP in a laboratory coordinate system. *X*-*Y* coupling is measured at each momentum deviation from the designed beam energy to obtain the chromatic *X*-*Y* coupling. By correcting chromatic *X*-*Y* coupling using skew sextupole magnets, it was found that the luminosity improved considerably by approximately 20%, and the highest luminosity of $2.108 \times 10^{34}\ \mathrm{cm}^{-2}\,\mathrm{s}^{-1}$ was achieved in June 2009.

In this paper, we present the measurements of chromatic *X*-*Y* coupling and the results of corrections carried out using skew sextupole magnets.

II. DEFINITION OF *X*-*Y* COUPLING

Even though, there is a linear coupling formalism [9], the notations and sign conventions used here are slightly different. Since a particle motion inside a solenoid field at the IP is treated, the linear analysis of a coupled lattice is based on a canonical transformation. The canonical momenta normalized by a design momentum are defined by

$$p_x = (1+\delta)x' - \frac{B_z}{2B\rho_0}y \qquad p_y = (1+\delta)y' + \frac{B_z}{2B\rho_0}x, \tag{1}$$

where $\delta = \Delta p/p_0$ is the momentum deviation, and B_z is a solenoid field along a beam axis. Here, the solenoid field is uniform and parallel to the beam axis.

In an *X*-*Y* decoupled coordinate system, the canonical variables of a particle can be expressed as

$$\begin{pmatrix} X \\ P_X \\ Y \\ P_Y \end{pmatrix} = \begin{pmatrix} \mu & 0 & -r_4 & r_2 \\ 0 & \mu & r_3 & -r_1 \\ r_1 & r_2 & \mu & 0 \\ r_3 & r_4 & 0 & \mu \end{pmatrix} \left\{ \begin{pmatrix} x \\ p_x \\ y \\ p_y \end{pmatrix} - \begin{pmatrix} \eta_x \\ \eta_{p_x} \\ \eta_y \\ \eta_{p_y} \end{pmatrix} \delta \right\}, \tag{2}$$

where (x, p_x, y, p_y) are the dynamical variables in a laboratory coordinate system and $(\eta_x, \eta_{p_x}, \eta_y, \eta_{p_y})$ is a disper-

*yukiyoshi.onishi@kek.jp

sion function in the horizontal and vertical plane. We refer to (r_1, r_2, r_3, r_4) as the *X*-*Y* coupling parameters, and the relationship between μ and the *X*-*Y* coupling parameters is expressed as

$$\mu^2 + (r_1 r_4 - r_2 r_3) = 1. \tag{3}$$

The *X*-*Y* coupling parameter is defined at each point along the beam orbit. If there is no *X*-*Y* coupling, the coupling parameters r_1, r_2, r_3, and r_4 are all zero. The canonical 4×4 transform matrix from location 1 to location 2 in the laboratory coordinate system, T_{21}, is expressed as

$$R_2 T_{21} R_1^{-1} = M_{21}, \tag{4}$$

where R_1 and R_2 are the *X*-*Y* coupling matrices at locations 1 and 2 defined in Eq. (2), and M_{21} is the transfer matrix in the decoupled coordinate system. Twiss parameters [10] are defined in the matrix M_{21}.

III. MEASUREMENT OF *X*-*Y* COUPLING

When only one mode is excited, the phase space of the beam attributed to a betatron oscillation in the laboratory coordinate system can be obtained by

$$x = \mu X \qquad p_x = \mu P_X \qquad y = -r_1 X - r_2 P_X \qquad p_y = -r_3 X - r_4 P_X \tag{5}$$

for H-mode ($Y = 0$, $P_Y = 0$) or

$$x = r_4 Y - r_2 P_Y \qquad p_x = -r_3 Y + r_1 P_Y \qquad y = \mu Y \qquad p_y = \mu P_Y \tag{6}$$

for V-mode ($X = 0$, $P_X = 0$). In the case of the H-mode, the *X*-*Y* coupling parameters are derived by Eq. (5) as

$$\begin{pmatrix} r_1 \\ r_2 \end{pmatrix} = -\frac{1}{\mu}\Sigma^{-1}\begin{pmatrix} \langle xy \rangle \\ \langle p_x y \rangle \end{pmatrix} \tag{7}$$

and

$$\begin{pmatrix} r_3 \\ r_4 \end{pmatrix} = -\frac{1}{\mu}\Sigma^{-1}\begin{pmatrix} \langle x p_y \rangle \\ \langle p_x p_y \rangle \end{pmatrix}, \tag{8}$$

where the envelope matrix is

$$\Sigma = \begin{pmatrix} \langle x^2 \rangle & \langle x p_x \rangle \\ \langle x p_x \rangle & \langle p_x^2 \rangle \end{pmatrix}. \tag{9}$$

The *X*-*Y* coupling parameters can be derived from the beam oscillations with consecutive turns in the laboratory coordinate system. We use the free oscillations of either of the two betatron normal modes (H-mode or V-mode) induced by a kicker. The beam centroid position on two orthogonal coordinates is measured using two turn-by-turn BPMs, which are located on either side of the IP behind a pair of final superconducting quadrupole magnets (QCS-L, QCS-R). The distance between the BPM and the IP is 2.49 m for the left side of the IP and 3.33 m for the right side in LER, 2.41 m for the left side of the IP and 3.37 m for the right side in HER, respectively. The accuracy of the beam position measured using tune-by-turn BPMs is typically 100 μm.

Assuming the transfer matrix of the model lattice in the laboratory coordinate system, which is defined by Eq. (4), we can reconstruct the phase space at the IP as follows:

$$\begin{pmatrix} x \\ p_x \\ y \\ p_y \end{pmatrix}_{\mathrm{IP}} = \begin{pmatrix} m_{11} & m_{12} & m_{13} & m_{14} \\ m_{31} & m_{32} & m_{33} & m_{34} \\ n_{11} & n_{12} & n_{13} & n_{14} \\ n_{31} & n_{32} & n_{33} & n_{34} \end{pmatrix} \begin{pmatrix} x_L \\ y_L \\ y_R \\ y_R \end{pmatrix}, \tag{10}$$

where m_{ij} and n_{ij} are the ijth elements of the transfer matrix from the IP to the left-side and the right-side BPM, respectively, (x_L, y_L) is the measured beam position at the left-side BPM, and (x_R, y_R) is the measured beam position at the right-side BPM. We calculate the model lattice with SAD [11], which is a computer code for the accelerator design developed at KEK.

We use the H-mode to measure the *X*-*Y* coupling parameters. A horizontal injection kicker is used to induce betatron oscillations in the horizontal plane. Then, we measure the vertical beam oscillations resulting from *X*-*Y* coupling and the rotation of the horizontal kicker around the beam axis. The difference between the horizontal and vertical betatron tunes can distinguish the beam oscillation caused by *X*-*Y* coupling from the kicker rotation. When we fit the turn-by-turn beam position in the vertical plane by using the horizontal tune frequency, the undesired contribution originating from the V-mode can be rejected. The horizontal betatron oscillation resulting from *X*-*Y* coupling at the BPMs caused by the vertical betatron oscillation is the second-order effect and can be ignored. We did not detect the horizontal oscillation because of the indirect V-mode described above in the measurement.

Prior to reconstructing the phase space at the IP, beam positions are fitted at each turn-by-turn BPM in order to extract a betatron motion by

$$\tilde{x}_{L,R} = x_{L,R} e^{-\Gamma n} \tag{11}$$

$$\tilde{y}_{L,R} = (y_{L,R} + y_{L,R}^{\mathrm{kicker}}) e^{-\Gamma n}, \tag{12}$$

where n is a turn number, the vertical oscillation caused by the kicker rotation is denoted by $y_{L,R}^{\mathrm{kicker}}$, and

$$x_{L,R} = \mu\sqrt{2J_x \beta_{x(L,R)}}\cos(2\pi\nu_x n + \psi_{x(L,R)}) \tag{13}$$

$$\begin{aligned} y_{L,R} &= -r_{1(L,R)} X_{L,R} - r_{2(L,R)} P_{X(L,R)} \\ &= W_{L,R}\sin(2\pi\nu_x n + \phi_{x(L,R)}) \end{aligned} \tag{14}$$

$$y_{L,R}^{\mathrm{kicker}} = \mu\sqrt{2J_y \beta_{y(L,R)}}\cos(2\pi\nu_y n + \psi_{y(L,R)}). \tag{15}$$

The radiation damping time is approximately 43 ms (46 ms) which corresponds to 4300 turns (4600 turns) in

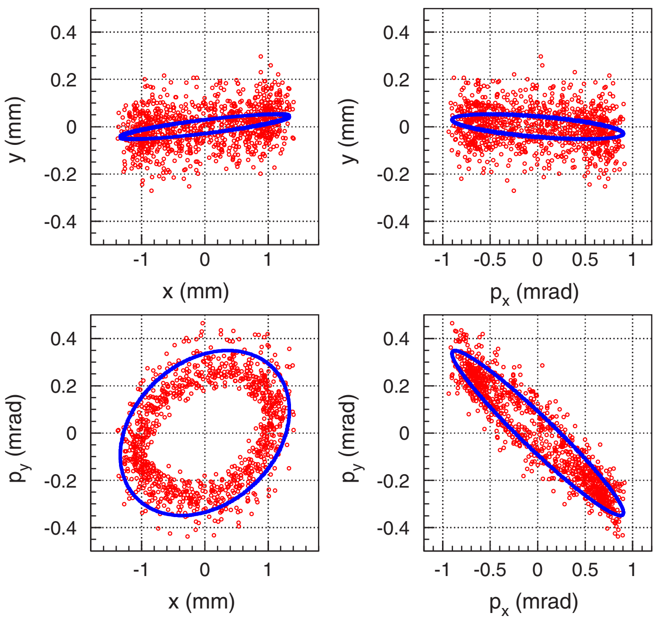

FIG. 1. (Color) Measured phase space plots at the IP in HER. Plots represent the raw data reconstructed by two turn-by-turn BPMs. The ellipse indicated by blue color is obtained from a result of fitted beam positions at the BPMs by 1000 consecutive turns.

LER (HER); the nonlinear effects are very small, and the damping rate resulting from the smearing effect is lower than $1/10$ of radiation damping. Besides nonlinearity, a head-tail effect affects the damping rate. The chromaticity is adjusted to be 1–3 typically, and the bunch current is 0.5 mA during the measurement. Consequently, the damping rate Γ is approximately (3–4) $\times 10^{-4}$, which is greater than 1000 turns used in the analysis.

Figure 1 shows a phase space plot at the IP in HER. In the case of the H-mode, a slant of the ellipse in the $x - y$ plot, $p_x - y$ plot, $x - p_y$ plot, and $p_x - p_y$ plot corresponds to r_1, r_2, r_3, and r_4 derived from Eq. (5), respectively. There is an ambiguity in μ; however, the *X*-*Y* coupling parameters, especially r_1 and r_2, are smaller than 0.1 in a normal condition, and we assume that $\mu = 1$ in this analysis.

Another uncertainty is the rotation of the BPMs around the beam axis to obtain the absolute values of the *X*-*Y* coupling parameters. In the case of chromatic *X*-*Y* coupling, a relative value is valid, and the rotation error of the BPMs is negligible for the measurements. The gain of the signals from the BPMs does not affect the measurement of *X*-*Y* coupling.

In order to check the validity of *X*-*Y* coupling measured by this technique, we compared the measured values with those changed by an IP tilt knob. The IP tilt knob controls the *X*-*Y* coupling parameters at the IP by using local bump orbits at a pair of sextupole magnets. Since the KEKB lattice adopts a noninterleaved sextupole chromaticity correction and a pair of sextupole magnets are connected by

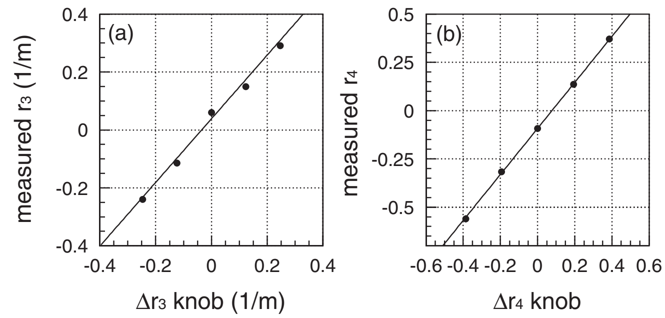

FIG. 2. Measured r3 (a) and r4 (b) at the IP as functions of a tilt knob in HER.

$-I'$ transfer matrix, a symmetric bump orbit at sextupole magnets in the vertical plane causes *X*-*Y* coupling at the IP without inducing a vertical dispersion in principle. The matrix $-I'$ is a 4 by 4 matrix similar to a negative identical transformation and the 12th and the 34th elements of the matrix are arbitrary.

The *X*-*Y* coupling parameters (r_1, r_2, r_3, r_4) are adjusted by the height of the bump orbit at four pairs of sextupole magnets, which are located on both sides of the IP. A comparison between the measured *X*-*Y* coupling parameters and the variations caused by the IP tilt knob in HER are shown in Fig. 2. In this figure, the coefficient of the line fitted by measurements is 1.10 ± 0.02 for r_3 and 1.19 ± 0.02 for r_4. In the case of LER, the coefficient is 1.11 ± 0.03 for r_3 and 0.98 ± 0.04 for r_4. A good linearity for the relationship between the measurement and the IP tilt knob is found from these results.

The measurements of r_1 and r_2 are related to the vertical oscillation caused by *X*-*Y* coupling. The amplitude of the vertical oscillation is weighted by the square root of the vertical beta function. In general, the vertical beta function at the IP is small for a collider such as KEKB. Conversely, p_y at the IP, which is sensitive to r_3 and r_4, is proportional to the inverse of the square root of the vertical beta function. r_1 and r_2 are sensitive to luminosity and are well optimized to be considerably small. The range of the IP tilt knob for r_1 and r_2 is smaller than the accuracy of r_1 and r_2 measurements restricted by the position resolution determined using the turn-by-turn BPMs.

IV. MEASUREMENT OF CHROMATIC *X*-*Y* COUPLING

The momentum of the beam in LER and HER is shifted by changing the rf frequency of the accelerating cavities to measure the *X*-*Y* coupling with the momentum deviation, $\Delta p/p_0$. The frequency of the rf cavity is 509 MHz, and the momentum compaction is typically $+3 \times 10^{-4}$ in the KEKB ring. The chromatic *X*-*Y* coupling is measured with seven different frequency shifts of -300, -200, -100, 0, $+100$, $+200$, and $+300$ Hz, which correspond to the range of $\pm 1.7 \times 10^{-3}$ for the momentum deviation.

TABLE I. Natural chromatic *X-Y* coupling estimated using the model lattice by SAD. Errors are the rms of the deviations obtained from the lattice simulation and include a rotation error of each normal sextupole magnet (see text).

	LER	HER
$\partial r_1/\partial\delta$	-0.059 ± 0.006	-0.207 ± 0.007
$\partial r_2/\partial\delta$ (m)	$+0.048 \pm 0.007$	$+0.266 \pm 0.009$
$\partial r_3/\partial\delta$ (1/m)	$+33.03 \pm 1.35$	$+38.61 \pm 1.05$
$\partial r_4/\partial\delta$	-30.48 ± 0.99	-132.54 ± 1.71

We calculate a transfer matrix from the turn-by-turn BPMs to the IP at each momentum deviation, and then, a phase space at the IP is reconstructed to determine chromatic *X-Y* coupling. Table I shows the natural chromatic *X-Y* coupling calculated using the model lattice.

In order to correct chromatic *X-Y* coupling, we use four pairs of skew sextupole magnets in LER and ten pairs are used in HER. Each skew sextupole magnet is installed in the vicinity of the normal sextupole magnets. The normal sextupole magnets are used to correct the natural chromaticity and determine the chromatic Twiss parameter at the IP. The location of the skew sextupole magnets is chosen to enable maximum scattering of their betatron phase advances. Figures 3 and 4 show the measured chromatic *X-Y* coupling in HER and LER, respectively. The plots indicated by blue color show *X-Y* coupling as a function of the momentum deviation when the skew sextupole magnets are turned off. On the other hand, the chromatic *X-Y* coupling corrected by the skew sextupole magnets is indicated by the color red. The plots are fitted by the third-order polynomial to obtain the chromatic *X-Y* coupling. In these figures, the dashed lines show the natural chromatic *X-Y* coupling (skew sextupole turned off), which is estimated using the model lattice by SAD. It is found that the second-order chromatic term is observed in the real lattice. The second-order chromatic term originates from the magnet configuration of the skew sextupole magnets. If there are enough skew sextupole magnets, the higher order chromatic *X-Y* coupling would be corrected. Results of the measured chromatic *X-Y* coupling parameters with/without the skew sextupole correction are listed in Table II.

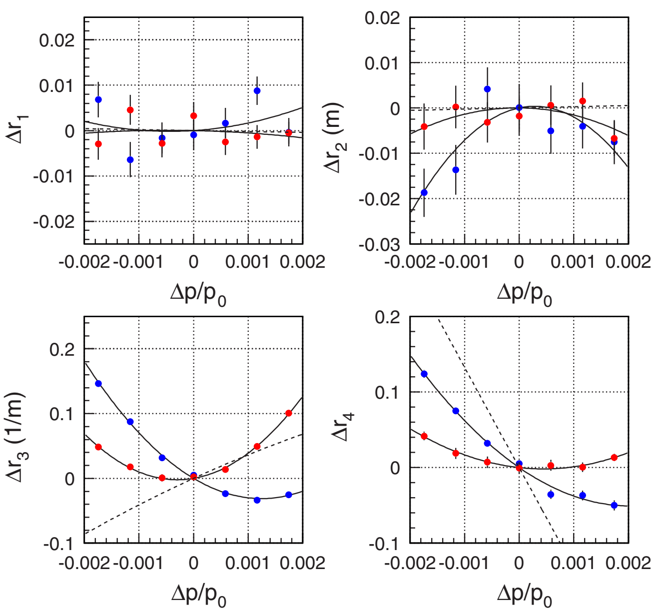

FIG. 3. (Color) Measured chromatic *X-Y* coupling at IP in HER. The blue plots indicate those before and the red plots indicate those after the skew sextupole correction. The dashed line indicates the natural chromatic *X-Y* coupling estimated using the model lattice by SAD.

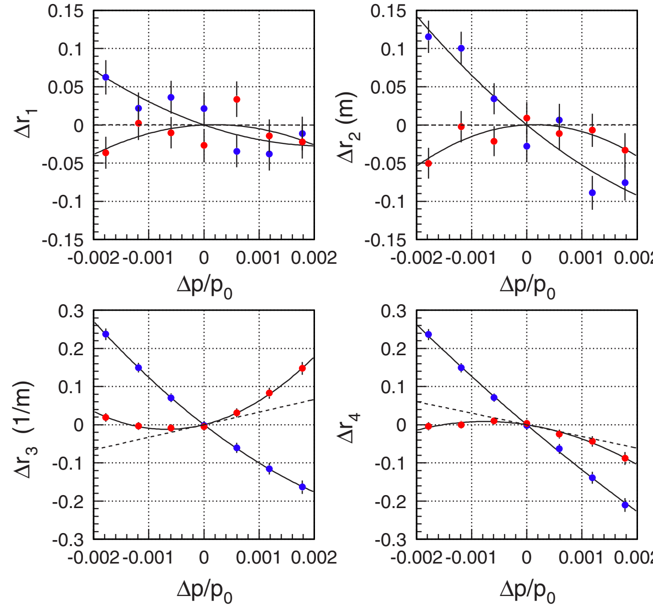

FIG. 4. (Color) Measured chromatic *X-Y* coupling at IP in LER. The blue plots indicate those before and the red plots indicate those after the skew sextupole correction. The dashed line indicates the natural chromatic *X-Y* coupling estimated using the model lattice by SAD.

V. CONCLUSION

We have measured chromatic *X-Y* coupling at the IP in both HER and LER at KEKB. The *X-Y* coupling parameters are derived from the analysis of the phase space structure, which is reconstructed using measured beam positions by turn-by-turn BPMs. Beam oscillation is a free oscillation with a damping time, which is induced by a horizontal kicker. The difference between the chromatic *X-Y* coupling of the model lattice and the measurements implies that a machine error caused by the rotation of the normal sextupole magnets around the beam axis and/or a skew multipole field originates from the final focus quadrupole magnet (QCS) and the IR special magnets cannot be ignored. We have investigated the machine error contributed by the rotation error of the normal sextupole magnets by carrying out lattice simulation. An rms of 0.2 mrad,

TABLE II. Measured chromatic *X*-*Y* coupling. Skew sextupole corrections are turned off and on.

	LER		HER	
Skew sextupole	Off	On	Off	On
$\partial r_1/\partial\delta$	-24.9 ± 7.0	$+3.1 \pm 6.9$	$+0.8 \pm 1.1$	-0.3 ± 1.0
$\partial r_2/\partial\delta$ (m)	-58.8 ± 7.0	$+3.3 \pm 6.8$	$+2.5 \pm 1.7$	-0.1 ± 1.5
$\partial r_3/\partial\delta$ (1/m)	-111.9 ± 4.8	$+35.8 \pm 4.3$	-50.1 ± 1.2	$+14.5 \pm 1.2$
$\partial r_4/\partial\delta$	-122.6 ± 4.8	-22.4 ± 4.2	-49.9 ± 1.8	-7.9 ± 1.9

which obeys a Gaussian distribution, is considered to be the rotation error. We generated and tested 1000 samples with a different random seed. The magnitude of the error indicates the alignment [12] of the magnets measured at KEKB. The deviations from the ideal model lattice are also shown as errors in Table I. From the result of the lattice simulation, it was found that the machine error caused by the rotation of the sextupole magnets is estimated to be smaller than ~10%; therefore, it is expected that the dominant error originates from the IR special magnets and the final focus quadrupole magnet. However, we can correct chromatic *X*-*Y* coupling by using skew sextupole magnets. The chromatic *X*-*Y* coupling is decreased by 3–6 times as shown in Table II and the luminosity gain of 20% has been achieved as the result of the skew sextupole correction. We conclude that the correction of chromatic *X*-*Y* coupling at the IP improves the luminosity, which is predicted by the beam-beam simulation.

ACKNOWLEDGMENTS

We thank the entire KEKB accelerator group for supporting the development of the technique used for the analysis. We also thank Dr. David Rice and Dr. Eugene Perevedentsev for their helpful discussions and encouragement.

[1] KEKB B-Factory Design Report, KEK Report No. 95-7, 1995.

[2] S. Kurokawa *et al.*, KEK Report No. 2001-157, 2001.

[3] H. Koiso, A. Morita, Y. Ohnishi, and K. Oide, in *Proceedings of the 2007 Particle Accelerator Conference, Albuquerque, New Mexico, 2007* (IEEE, Albuquerque, New Mexico, 2007), THPAN042.

[4] A. Morita, H. Koiso, Y. Ohnishi, and K. Oide, Phys. Rev. ST Accel. Beams **10**, 072801 (2007).

[5] D. Zhou, K. Ohmi, Y. Seimiya, Y. Ohnishi, and A. Morita, KEK Report No. 2009-10, 2009.

[6] Y. Seimiya, H. Koiso, and K. Ohmi, in Particle Accelerator Conference PAC09, 2009, Vancouver, Canada, TH6PF080.

[7] D. Sagan, R. Miller, R. Littauer, and D. Rubin, Phys. Rev. ST Accel. Beams **3**, 092801 (2000).

[8] Y. Cai, Phys. Rev. E **68**, 036501 (2003).

[9] D. Sagan and D. Rubin, Phys. Rev. ST Accel. Beams **2**, 074001 (1999).

[10] E. D. Courant and H. S. Snyder, Ann. Phys. (Paris) **3**, 1 (1958).

[11] Strategic Accelerator Design, http://acc-physics.kek.jp/SAD.

[12] M. Masuzawa and R. Sugahara, KEK Report No. 2003-97, 2003.